

## Plastronic Circular Line Matched Dipole Antenna

Gildas Bengloan<sup>1, 2, \*</sup>, Anne Chousseaud<sup>1</sup>, Bruno Froppier<sup>1</sup>, Jacques Girard<sup>2</sup>,  
Marc Brunet<sup>1</sup>, and Eduardo M. Cruz<sup>1</sup>

**Abstract**—A compact 3-D, circular line matched dipole (CLMD) antenna is presented in this paper. The realization of the antenna is based on Laser Direct Structuring (LDS) plastronic technology, enabling metallization on plastic parts. Cylindrical holder is chosen to carry the dipole, which implies high bending constraints on the antenna. Miniaturization of the radiating element is obtained by an effective use of 3-D space, resulting in a very low profile length dimensions of  $0.14\lambda \times 0.14\lambda \times 0.05\lambda$  operating at 868 MHz. Specific attention is paid to the input impedance change due to conformation. An equivalent circuit model is proposed to take into account the conformation and design the matching line. Both simulated and measured results demonstrate good performances, with a 30 MHz bandwidth (i.e., a relative bandwidth of 3.5% with  $S_{11} < -10$  dB) around the working frequency. The LDS prototype achieves a maximum gain of 1.2 dBi with a quasi-omnidirectional radiation pattern. This compact and conformal design presents a real interest for pervasive highly integrated ISM band IoT sensors.

### 1. INTRODUCTION

In the last decade, the development of research in Internet of Things (IoT) has established the major communications protocols for Low Power Wide Area Network (LPWAN). These standards include LoRa and SigFox in the sub-GHz Industrial, Scientific and Medical (ISM) band between 863 MHz and 930 MHz. They are particularly well suited for IoT purposes and come out as two of the most used Wireless Sensor Network protocols. Low data load, low rate, and long range are accompanied by the exponential growth of the number of connected devices through the years. This increase is accompanied by the need of more pervasive, energy-efficient, and compact sensor solutions. Indeed, many applications related to the IoT require the use of small devices, such as smartwatch, highly integrated sensors, and telemetry probes. In the context of Industry 4.0, the proliferation of connected devices will allow real-time management and modification of the production tool and better control of the Supply Chain. Nonetheless, considering the frequency dedicated to the ISM band protocol (860 MHz to 930 MHz), antenna size is a hindrance to the compactness criterion.

Many solutions have been proposed in the past for antenna size reduction. Folding or meandering of classic antenna shapes, like inverted-F antenna (IFA), monopoles, and dipoles are interesting ways to reduce antenna space [1]. However, they often degrade the bandwidth of the radiating element and may sometimes require a bulky ground plane to be effective [2]. Inductive or capacitive loading is also used for the miniaturization [3]. By using particular elements such as inter-digital lines or inductive slots, the antenna impedance is controlled to achieve a miniaturization through reactance cancellation. Magneto-dielectric material, high permittivity substrate, and meta-material are as well common methods for achieving compact antennas [4]. Nevertheless, these techniques tend to increase the stored energy in the antenna thus its Q-factor, resulting in very short bandwidth and poor radiative antennas. According

---

*Received 12 May 2021, Accepted 11 June 2021, Scheduled 24 June 2021*

\* Corresponding author: Gildas Bengloan (gildas.bengloan@univ-nantes.fr).

<sup>1</sup> Univ Nantes, CNRS, IETR UMR 6164, Nantes, France. <sup>2</sup> LACROIX Impulse, 13 rue Claude Chappe, Cesson-Sévigné 35510, France.

to [5], one of the most effective techniques to ally antenna compactness and performances is to fit within the smallest sphere containing the antenna as well as possible. Such a 3-D folded antenna configuration provides the lowest quality factor, highest bandwidth, and radiation efficiency in comparison to planar developments.

With the aim of reducing antenna size for IoT purpose, plasronics appears as a good candidate, combining plasturgy and electronics conceptions in order to lead to an efficient use of 3-D space. Although plasronics is initially a circuit-oriented domain, it also provides alternatives for antenna miniaturization. In most cases, this technology permits to avoid having to devote space on the electronic board for the antenna. This leads to an electronic board size reduction, thus an overall size reduction of the product. Among all the plasronics technologies, Laser Direct Structuring offers promising results for IoT developments [6–8]. Indeed, considering the aim to produce a serial antenna, the Laser Direct Structuring (LDS) process offers both sufficient flexibility in the prototyping phase and convenient integration of the different stages in a single industrialization process. Moreover, this technology provides very interesting manufacturing costs for large production volumes. Some other technologies could have been considered in the development, such as inkjet printing or flexible Printed Circuit Boards (FPCB). Firstly, inkjet printing has shown good results in terms of bandwidth and radiation efficiency for IoT dedicated flexible antenna [9]. However, in order to avoid micro-cracking in the metallization, this technology is rarely subjected to bending stresses as strong as those of the present study. Secondly, FPCB antennas demonstrate satisfying performances for compact and conformal applications in an industrial context [10]. Nevertheless, the thinness of the available flexible substrates can lead to difficulties in the design of feed lines, especially in managing the characteristic impedance. In addition, both technologies require the production and assembly of different parts (paper or flexible PCB substrates), while LDS directly customizes the plastic part as a unique component. As a result, the LDS assembly requirements are reduced, which lowers production costs. In this work, a bowtie dipole antenna with a circular matching line is designed on a cylindrical substrate. LDS technology is used for the fabrication. A preliminary study is carried out to highlight the effect of conformation on the antenna impedance. The different steps of LDS antenna conception and measurements are then presented.

## 2. ANTENNA DESIGN

The proposed dipole antenna is dedicated to be mounted on a plastic holder of the kind one may find for industrial wall light fixtures. It consists of a quasi-cylindrical structure of radius 24 mm and 17 mm long. Earlier study on arc dipole antennas has shown that curving a dipole directly affects its input impedance  $Z_{in}$  [11]. A more recent paper has highlighted the impact of different curvature values  $K = 1/R$  on bent dipole performances, (where  $R$  is the radius of curvature of the dipole) [12]. It appears that above specific value of  $K > 3\pi/\lambda$ , the antenna exhibits poor adaptation and low radiation. For a dipole operating at 868 MHz, the theoretical curvature value for which the performances of the antenna are highly deteriorated is  $K > 27$ .

In the present study, the cylindrical holder has a radius of 24 mm, which imposes a value of  $K = 41.7$ . Thus, it is impossible to use a classical dipole configuration projected on the cylinder; otherwise, high performance degradation would occur, mainly due to impedance mismatch.

In others words, bent dipole antenna conception becomes only a matter of impedance matching capability. Numerous ways of antenna matching exist, although they are mainly used to match complex impedance while a specific chipset is dealt with. The well-known T-match structure presented in detail in [13] is one of the most common ways for antenna matching due to its relative simplicity. The loop structure and reversed T configurations are also good methods for this kind of operation [14, 15]. In this paper, the authors propose a simple way to match a bent dipole with a circular line. The antenna structure is presented in Fig. 1.

The antenna structure corresponds to a planar bow-tie dipole antenna projected on a quasi-cylindrical plastic body. Two parts of the holder make it not totally cylindrical. A top located chamfered area of  $19.3 \times 16.5 \text{ mm}^2$  is dedicated to a planar balun and the feeding structure. There is also a small chamfered area at the bottom of the holder as to ensure its placement in the wall light casing. Without any loss of considerations, we assimilate the plastic part as a perfect cylinder. Bow-tie shape has already

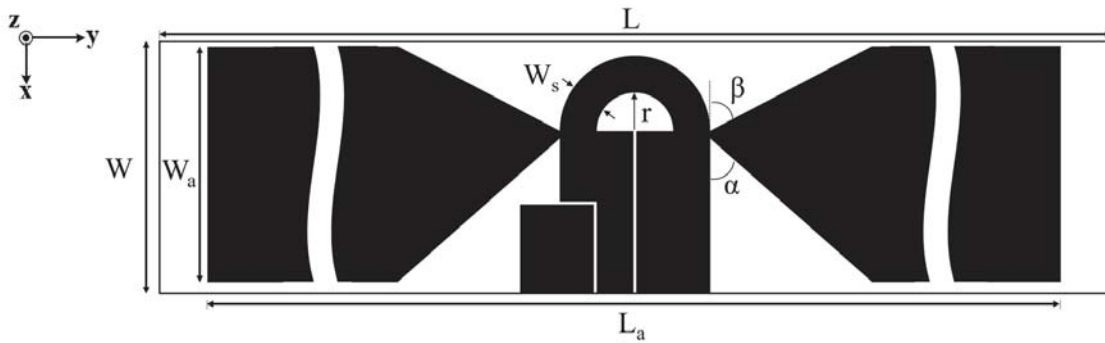


**Figure 1.** Circular Line Matched 3-D Dipole Antenna, planar projection.

been used for dipole on a cylinder, showing wider bandwidth and reducing the overall space needed in comparison with standard dipole [16]. In contrast to the previous study, the design is not dedicated to VHF arrays but UHF standalone antenna, and it does present an integrated impedance matching structure for  $50\ \Omega$  adaptation.

Standard balun solutions such as Marchand balun [17] or Y-junction [18] are relatively bulky because they require the use of a quarter-wave transmission line. Considering the limited space available for the antenna, these solutions were not selected. It is also impossible to use surface mount baluns as their height would prevent the plug from entering the light fixture. Consequently, a compact planar balun inspired from [19] and fed by a coplanar waveguide (CPW) transmission line is used. The CPW to coplanar stripline (CPS) transition is based on the concept of impedance matching between the two lines. Ensuring a good matching between them enables a maximum power transfer and limits return current to the feed. The project specifications for the measurements imply a CPW line characteristic impedance of  $50\ \Omega$ . Then, according to [20], the characteristic impedance of the CPS line can be selected between  $55\ \Omega$  and  $90\ \Omega$  for the transition. Given the accuracy of LDS technology, it is technically impossible to ensure a  $55\ \Omega$  impedance matching for the CPS line because of the fineness required for the line gap. The characteristic impedance of the CPS lines is then fixed at  $86\ \Omega$  using a gap of  $200\ \mu\text{m}$  and a line width of  $5\ \text{mm}$ . Measurements on back-to-back prototypes indicate that the transition transforms unbalanced to balanced modes with less than  $0.3\ \text{dB}$  transmission losses at  $868\ \text{MHz}$ . This compact antenna then includes both the radiating element and the balun.

The low profile circular line dedicated to the antenna matching links the two arms of the dipole, where dimensions do not exceed  $10 \times 7\ \text{mm}^2$ . The antenna dimensions are optimized by ANSYS High Frequency Structure Simulator (HFSS 17) software, in order to exhibit the wider bandwidth around the working frequency. The parameter values defined in Fig. 1 are listed as follows (unit: mm if not specified):  $L = 150$ ,  $W = 17$ ,  $L_a = 122$ ,  $W_a = 16$ ,  $W_s = 2.5$ ,  $r = 2.6$ ,  $\alpha = 48.5^\circ$ ,  $\beta = 62^\circ$ .

An equivalent circuit model is set up to bring out the circular line effect on the antenna behaviour. We first assume an antenna equivalent circuit model composed of an RLC tank in series with an inductor and a capacitor as described in [21].  $L_a$ ,  $C_a$ ,  $L'_a$ ,  $C'_a$ , and  $R_a$  represent the dipole parameters presented in the prior mentioned reference, and the circuit is outlined by a blue dotted line in Fig. 2. Bending the dipole does not change the equivalent model because the antenna pattern remains identical. However, it does modify the values of the components, which implies the input impedance shift highlighted in the aforementioned studies. Therefore, a dipole dimensioned for flat operation will be unsuitable when being used in a cylindrical projection. In this work, we propose a solution involving minor modifications to the original dipole in order to enable the adaptation once conformed. Moreover, this method does not affect the maximum gain achieved in comparison to standard dipole.

The circular line can be seen as an inductive matching circuit. Two components are used in order to modelize this matching circuit: one series and one parallel inductors, namely  $L_1$  and  $L_2$ . The matching circuit values are directly related to the width and radius of the circular line (resp.  $W_s$  and  $r$  in Fig. 1). A 3D circuit/EM co-simulation technique is employed with the aim of determining the values of  $L_1$  and  $L_2$  to match the equivalent circuit model to the 3D EM simulations. Variation of  $W_s$  mainly affects the reactance of the antenna, and when  $W_s$  increases the reactance does too. The radius  $r$  is used to adjust

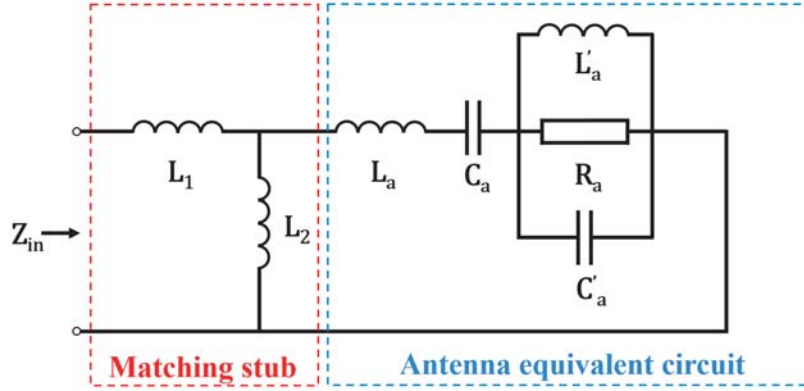


**Figure 2.** Equivalent circuit model of conformed dipole antenna with the circular line.

central frequency of the matching stub, and the larger it is, the lower the matching frequency is. From a circuit-equivalent point of view,  $L_1$  models the effect of  $W_s$ , and  $L_2$  the behaviour of  $r$ .

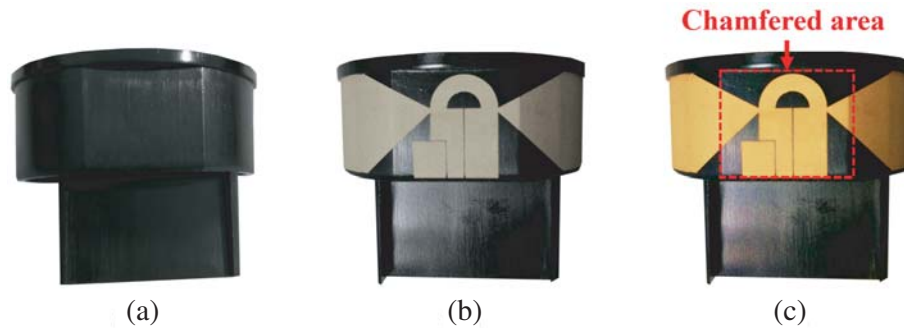
All the circuit values of the equivalent models are listed in Table 1. The equivalent circuit model gives an accurate estimation of the circular line matched dipole (CLMD) antenna return Loss over the whole frequency bandwidth studied here. The comparison between the circuit model, HFSS simulations, and measurements results is presented in the next section.

**Table 1.** Lumped elements equivalent circuit model values.

$L_a$	$C_a$	$R_a$	$L'_a$
30.52 nH	0.91 pF	34.75 $\Omega$	2.24 nH
$C'_a$	$L_1$	$L_2$	$Z_{in}$
3.84 pF	6.24 nH	5.54 nH	50 $\Omega$

### 3. RESULTS AND DISCUSSIONS

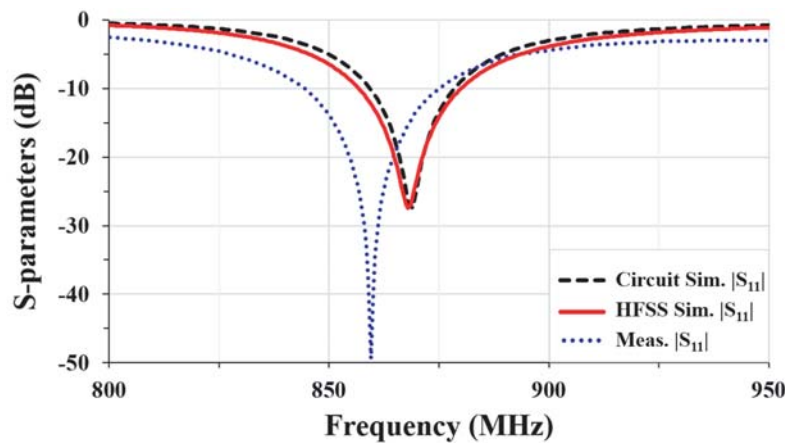
The plasmonic antenna fabrication with Laser Direct Structuring technology is composed of three steps, Fig. 3. In the first time, the cylindrical plastic holder is created by injection molding. Specific LDS-suitable polycarbonate thermoplastic Thermocomp DX11355 with a dielectric constant of 2.92 and loss tangent of 0.007 (at 1 GHz) is used for the injection. The plastic part is then cleaned in order to prepare the next step. Secondly, the antenna pattern is obtained by means of a specific laser beam.



**Figure 3.** LDS fabrication steps of the CLMD antenna: (a) plastic part; (b) activation; (c) metallization.

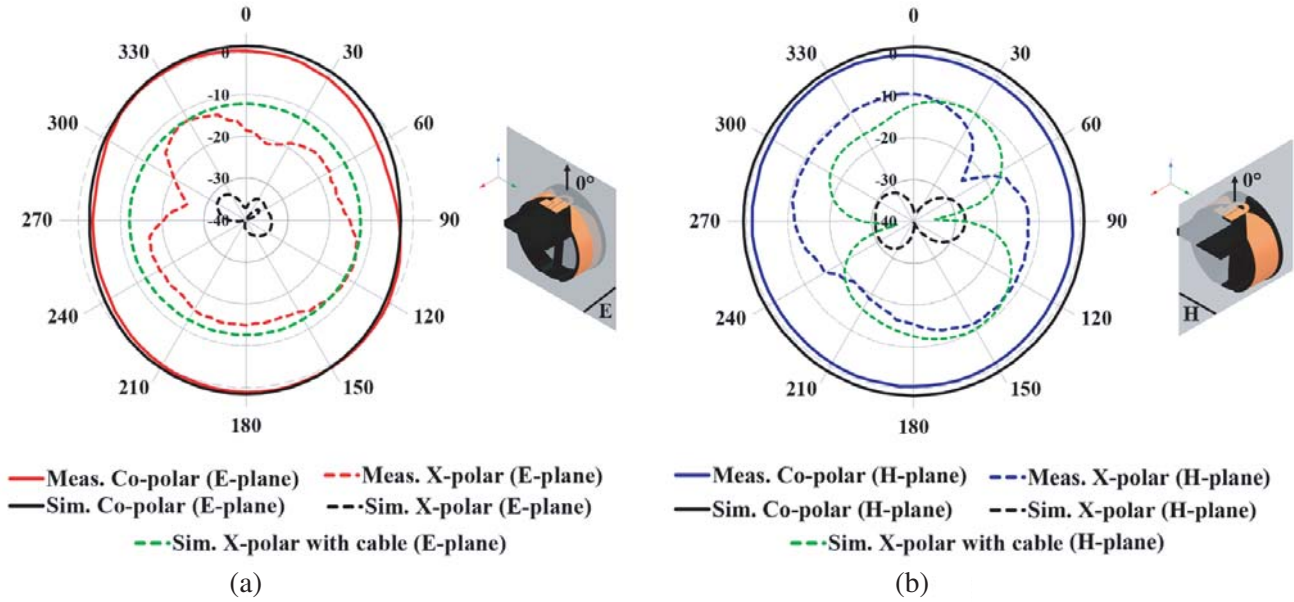
Laser activation induces a thin surface depletion and locally modifies the thermoplastic composition. This step allows electrolytic reaction on specific parts of the substrate. Finally, metal deposit is made by three chemical baths of copper, nickel, and gold. Spectroscopic measurements indicate average thicknesses of the three layers to be  $5.7\ \mu\text{m}$  copper,  $3.5\ \mu\text{m}$  nickel, and  $0.4\ \mu\text{m}$  gold. Multiple metallized areas were tested to ensure metal thickness uniformity all over the plastic part, resulting in an average thickness of  $9.6\ \mu\text{m}$ . A SubMiniature version A (SMA) connector is glued with a conductive paste for measurements as the thermoplastic used here does not stand high temperatures.

Figure 4 compares the measured, HFSS-simulated and equivalent circuit-simulated  $S$ -parameters of the CLMD antenna. Return Loss measurements were performed with a Rhode & Schwarz ZNB20 VNA using a TRL calibration. We first observe a good agreement between the circuit equivalent model of the antenna and the HFSS simulations results. The established model shows results in line with those of the 3-D electromagnetic solver. Hence, the series parallel inductors accurately describe the matching effect of the circular line. Then, a slight frequency shift of 1% is observed in measurements, as a working frequency of 860 MHz is obtained instead of 868 MHz. LDS fabrication tolerances and minor deviation of the thermoplastic dielectric constant might explain this phenomenon. However, this does not affect the LoRa operation capability, as the CLMD antenna exhibits a 30 MHz bandwidth. Consequently, a good matching is still found at 868 MHz ( $S_{11} < -10\ \text{dB}$ ).



**Figure 4.** Reflection coefficient of the CLMD antenna in measurements and simulation.

Radiation pattern measurements in free space were performed in a LACROIX Impulse anechoic chamber. Simulated and measured radiation patterns of the antenna at 868 MHz are presented in Fig. 5(a) and Fig. 5(b) for  $E$ -plane and  $H$ -plane, respectively. Additional measurements were carried out at the resonance frequency of the antenna, at 860 MHz, showing very similar results to those presented at 868 MHz. Good agreement with simulated data is found in both planes for co-polarization. The antenna has a maximum gain of 1.2 dBi in the  $E$ -plane and 0.2 dBi in the  $H$ -plane. In addition, a quasi-omnidirectional behaviour is found in the  $H$ -plane, making it suitable for IoT sensor nodes communications. It can be seen that the measured cross-polarization levels in both planes are higher than the simulated ones for the stand-alone antenna. It appears that the measuring cable significantly affects the cross component of the polarization. This well-known phenomenon is often encountered while dealing with compact balanced antenna measurements [22]. Although it correctly transforms CPW feed line to Coplanar Stripline (CPS), the selected balun causes a slight current leakage. Consequently, the antenna cable in measurements radiates a small amount of power, particularly noticeable for the cross-polarizations. Retro-simulations were carried out by taking into account the cable as to ensure this hypothesis. Black dashed lines of Fig. 5(a) and Fig. 5(b) correspond to the simulations results with a 200 mm cable feeding the antenna. This length is equivalent to that of the effective cable used in measurements. A good correlation is found while the cable effect is taken account. The cross-polarization components remain approximately 15 dB lower than co-polarization in the  $E$ -plane and 10 dB in the  $H$ -plane, which does not affect the antenna operation.



**Figure 5.** Measured and simulated radiation patterns of the CLMD antenna at 868 MHz (dBi): (a) *E*-plane; (b) *H*-plane.

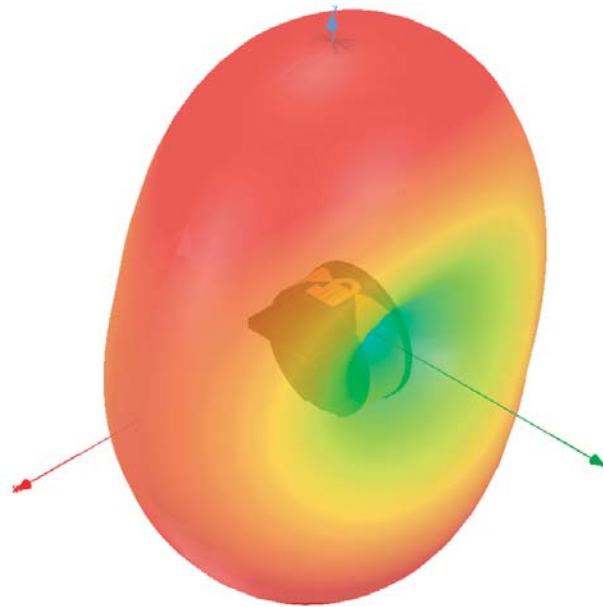


**Figure 6.** Simulated 3-D radiation pattern of the CLMD antenna at 868 MHz.

The 3-D radiation pattern of the CLMD antenna is shown in Fig. 6. It can be seen that the antenna radiates favourably in the direction of the *z*-axis, which corresponds to the desired direction of propagation in the use-case. In addition, lower radiation levels are found in the *y*-axis. That is to say, the antenna does have a conventional dipole radiation pattern with an ‘8’ shape in the *E*-plane and with a ‘0’ shape in the *H*-plane. This is not clearly shown in Fig. 5 because of the scale effect induced by the need to show the cross polarisations and their low level. Thus, it ensures the compatibility of the antenna solution, since the use-case will mainly exploit radiation from above or below the antenna.

#### 4. CONCLUSION

A circular line matched 3-D dipole antenna is proposed in this paper. Low-profile dimensions of  $0.14\lambda \times 0.14\lambda \times 0.05\lambda$  are obtained by an effective use of the available space by means of Laser Direct Structuring plasmonic technology. The compact matching structure permits the antenna operation despite the high constraints imposed by the bending. Using an equivalent-circuit model, we showed that the circular line could be assimilated as a matching circuit composed of one series and one parallel inductors. The antenna achieves a bandwidth of 30 MHz (3.5%) around the working frequency of 868 MHz. Good agreement is found between simulations and measurements, and a maximum gain of 1.2 dBi is obtained in  $E$ -plane. Despite a strong conformation, the low-profile antenna shows good performances for future IoT developments. To conclude, the cylindrical antenna topology used allows the control of sufficient bandwidth for LoRa protocols while ensuring low levels of cross polarisation. Consequently, the observations tend to conclude on a technological validation of the LDS for these types of constrained applications.

#### REFERENCES

1. Marrocco, G., "Gain-optimized self-resonant meander line antennas for RFID applications," *IEEE Antennas and Wireless Propagation Letters*, Vol. 2, 302–305, 2003.
2. Best, G. R. and J. D. Morrow, "On the significance of current vector alignment in establishing the resonant frequency of small space-filling wire antennas" *IEEE Antennas and Wireless Propagation Letters*, Vol. 2, 201–204, 2003.
3. Volakis, J., et al., *Small Antennas: Miniaturization Techniques and Applications*, McGraw-Hill, 2010.
4. Mosallei, H. and K. Sarab, "Engineered meta-substrates for antenna miniaturization," *Proc. 2004 URSI Int. Symposium on Electromagn. Theory*, 191–193, 2004.
5. Best, G. R. and J. M. MCGinthy, "A comparison of electrically small HF antennas," *2005 IEEE Antennas and Propagation Society International Symposium*, Vol. 1B, 37–40, 2005.
6. Kumar, H., et al., "A wristwatch-based wireless sensor platform for IoT health monitoring applications," *Sensors*, Vol. 20, 1675–1680, 2020.
7. Cihangir, A., et al., "Antenna solutions for 4G smartphones in laser direct structuring technology," *Radioengineering*, Vol. 25, 419–428, 2016.
8. Sonnerat, F., et al., "Innovative 4G mobile phone LDS antenna module using plasmonics integration scheme," *2013 IEEE Antennas and Propagation Society International Symposium (APSURSI)*, 2013.
9. Ahmed, S., F. Tahir, A. Shamim, and H. Cheema, "A compact Kapton-based inkjet-printed multiband antenna for flexible wireless devices," *IEEE Antennas and Wireless Propagation Letters*, Vol. 14, 1802–1805, 2015.
10. Wu, K., J. Sun, and G. Chen, "Flexible printed circuit board (FPC) antennas for mobile phone operation," *5th International Microsystems Packaging Assembly and Circuits Technology Conference*, 1–4, 2010.
11. Tang, C., "Input impedance of arc antennas and short helical radiators," *IEEE Transactions on Antennas and Propagation*, Vol. 1, 2–9, 1964.
12. Arumugam, D., et al., "The effect of curvature on the performance and readability of passive UHF RFID tags," *ACES Journal*, 2010.
13. Balanis, C. A., *Antenna Theory: Analysis and Design*, 3rd Edition, Wiley-Interscience, 2005.
14. Marrocco, G., "The art of UHF RFID antenna design: Impedance-matching and size-reduction techniques," *IEEE Antennas and Propagation Magazine*, Vol. 50, 66–79, 2008.
15. Wang, S., et al., "A novel reversed T-match antenna with compact size and low profile for ultrawideband applications," *IEEE Transactions on Antennas and Propagation*, Vol. 60, 4933–4937, 2012.

16. Gao, X., et al., "Conformal VHF log-periodic balloon antenna," *IEEE Transactions on Antennas and Propagation*, Vol. 63, 2756–2761, 2015.
17. Marchand, N., "Transmission line conversion transformers," *Electronics*, Vol. 17, 142–145, 1944.
18. Trifunovic, V. and B. Jokanovic, "Review of printed Marchand and double Y baluns: Characteristics and application," *IEEE Trans. Microwave Theory Tech.*, Vol. 42, 1454–1462, 1994.
19. Anagnostou, D. E., et al., "A 0–55-GHz coplanar waveguide to coplanar strip transition," *IEEE Transactions on Microwave Theory and Techniques*, Vol. 56, 1–6, 2008.
20. Chiou, H.-K., C.-Y. Chang, and H.-H. Lin, "Balun design for uniplanar broad band double balanced mixer," *Electronics Letters*, Vol. 31, 2113–2114, 1995.
21. King, R. W. P, *The Theory of Linear Antennas*, Harvard University Press, 1956.
22. DeMarinis, J., "The antenna cable as a source of error in EMI measurements," *IEEE 1988 International Symposium on Electromagnetic Compatibility*, 1988.